Journal of Radiation Research

OXFORD

Development of a minipig model for lung injury induced by a single high-dose radiation exposure and evaluation with thoracic computed tomography

Jong-Geol Lee[1], Sunhoo Park[1,2], Chang-Hwan Bae[1], Won-Suk Jang[1],
Sun-Joo Lee[1], Dal Nim Lee[1], Jae Kyung Myung[2], Cheol Hyeon Kim[3],
Young-Woo Jin[1], Seung-Sook Lee[1,2] and Sehwan Shim[1]*

[1]Laboratory of Radiation Exposure and Therapeutics, National Radiation Emergency Medical Center, Korea Institute of Radiological and Medical Sciences, 215–4, Gongneung-dong, Nowon-gu, Seoul, Republic of Korea
[2]Department of Pathology, Korea Cancer Center Hospital, KIRAMS, Seoul, Republic of Korea
[3]Division of Pulmonology, Department of Internal Medicine, Korea Cancer Center Hospital, KIRAMS, Seoul, Republic of Korea
*Corresponding author. Laboratory of Radiation Exposure and Therapeutics, National Radiation Emergency Medical Center, Korea Institute of Radiological and Medical Sciences, 215–4, Gongneung-dong, Nowon-gu, Seoul, 139–706, Korea. Tel: +82-2-970-1438; Fax: +82-2-970-1980; Email: ssh3002@kirams.re.kr
Received June 17, 2015; Revised October 20, 2015; Accepted October 23, 2015

ABSTRACT

Radiation-induced lung injury (RILI) due to nuclear or radiological exposure remains difficult to treat because of insufficient clinical data. The goal of this study was to establish an appropriate and efficient minipig model and introduce a thoracic computed tomography (CT)-based method to measure the progression of RILI. Göttingen minipigs were allocated to control and irradiation groups. The most obvious changes in the CT images after irradiation were peribronchial opacification, interlobular septal thickening, and lung volume loss. Hounsfield units (HU) in the irradiation group reached a maximum level at 6 weeks and decreased thereafter, but remained higher than those of the control group. Both lung area and cardiac right lateral shift showed significant changes at 22 weeks post irradiation. The white blood cell (WBC) count, a marker of pneumonitis, increased and reached a maximum at 6 weeks in both peripheral blood and bronchial alveolar lavage fluid. Microscopic findings at 22 weeks post irradiation were characterized by widening of the interlobular septum, with dense fibrosis and an increase in the radiation dose–dependent fibrotic score. Our results also showed that WBC counts and microscopic findings were positively correlated with the three CT parameters. In conclusion, the minipig model can provide useful clinical data regarding RILI caused by the adverse effects of high-dose radiotherapy. Peribronchial opacification, interlobular septal thickening, and lung volume loss are three quantifiable CT parameters that can be used as a simple method for monitoring the progression of RILI.

KEYWORDS: Göttingen minipigs, radiation, lung injury, computed tomography

INTRODUCTION

Lung injury was identified as an important area of interest in radiation research after a significant number of victims died early from radiation-induced lung injury (RILI) after the Chernobyl accident [1]. When investigating the manifestations of RILI and developing treatment strategies, ability to quantify the pathological progression of lung fibrosis induced by radiation exposure is of critical importance. However, clinical data on RILI have been very limited because of the rarity of cases and the ethical limitations of clinical trials using humans [2–4].

Researchers investigating lung diseases have used a wide variety of animal models, and a significant majority of them have used rodents

[5, 6]. However, the pathology of the rodent lung is quite different from that of the human lung in terms of lobularity, the thickness of the septa and pleura, and the blood supply to the pleura [1, 7]. Therefore, it is necessary to develop an alternative animal model that appropriately mimics the human response to radiation in order to investigate RILI.

The two major candidates for an alternative animal model, the dog and the non-human primate, have advantages and disadvantages for radiation lung studies. Specifically, the lung of the dog differs from that of the human, and shares similarities in pulmonary anatomy and function with rodent lungs [7]. Despite the similarities of non-human primate physiology to human physiology, few investigators have used the non-human primate to study radiation effects in the lung [1].

The similarities in anatomy and pathology between pig and human lungs make the pig model particularly useful for translational respiratory medicine [8–20]. The size of the pig also allows testing of many interventions used in humans. The pig model is a well-known large animal model for scientific and medical studies for radiation-induced bone marrow, skin, gastrointestinal and glandular injury [21–29]. For these reasons, we chose to investigate the pig as a model for RILI.

The methods for *in vivo* lung procedures in the pig have rarely been described. Some groups have used breathing rates to assess pneumonitis [30], but had limited success in monitoring fibrosis. Some groups have measured cytokine and growth factor expression induced in the lung after irradiation [31, 32], although none of the cytokines or growth factors evaluated have been shown to directly cause lung injury.

Chest computed tomography (CT) has been introduced as a radiological diagnostic method for detecting lung abnormalities [33]. It is safe, non-invasive and widely accessible, making it well suited for clinical implementation, and its distinct patterns for lung injury have been previously described from the lungs of humans receiving radiotherapy [34]. Some groups have used CT previously [35, 36], but limitations of studies to date include largely qualitative radiologic interpretation, diagnostic variability among observers, and the necessity for specialized expertise [37–40]. For the objective quantitative analysis of lung injury progression by thoracic CT, measurement of Hounsfield units (HU) and 3D reconstruction from thoracic CT sections have been used to assess the changes in lung density and volume, respectively. However, in the case of 3D reconstruction of the lungs, processing requires multiple steps, is time-consuming [41–43], and other than HU measurement, lacks easily quantifiable parameters. Therefore, we explored simple, easy and quantitative parameters for RILI, including a slightly modified translation of HU measurement (using thoracic CT scans in order to accelerate the evaluation of lung injury progression in our minipig model, without specialized expertise).

The goal of the current study was to describe the use of an optimal minipig model for assessing RILI induced by a single high-dose radiation exposure, and to evaluate RILI progression via a thoracic CT technique employing novel quantitative parameters.

MATERIALS AND METHODS
Animals
Male Göttingen minipigs (PWG Genetics Korea, PyungTek, Korea) weighing 15–20 kg were used in this study. Prior to purchase, the pigs were physically examined and determined to be healthy. Pigs were housed indoors in individual cases, fed dry pig food and provided with triple-filtered water. The animals were housed under environmentally controlled conditions at 22 ± 1°C and 50 ± 10% relative humidity, with 12-h light/dark cycles throughout the experimental period. All animal experiments were approved by the Animal Investigation Committee of the Korea Institute of Radiological and Medical Sciences (KIRAMS).

Irradiation protocol
Six minipigs were anesthetized with an intramuscular injection of 3 mg/kg of tiletamine/zolazepam (Zoletil 50®; Virbac, Republic of Korea) and 0.06 mg/kg medetomidine (Domitor®' Pfizer Animal Health, Republic of Korea). Precise localization of whole right lung lobes for determining irradiation fields was performed under chest X-ray guidance (SM-20HF, Listem, Seoul, Korea). Subsequently, the whole right hemithorax was irradiated with 0, 25 or 30 Gy (*n* = 2 per group). For irradiation, the minipigs were placed in the prone position and irradiated in a ^{60}Co gamma-ray irradiation unit (Theratron 780, AECL, Ontario, Canada); the average calculated dose rate at the center of the field was 143.17 cGy/min. The distance between the source of radiation and the thoracic skin was 80 cm. After irradiation, pigs were housed individually, fed dry pig food and provided with triple-filtered water under environmentally controlled conditions.

Thoracic computed tomography
The acquisition of all CT images was performed in the Ian Animal Diagnostic Imaging Center (Seoul, Korea) at 6, 12, 17 and 22 weeks after irradiation. Briefly, thoracic CT scanning was performed using a multi-detector-row CT unit (Asteion Super 4; Toshiba, Tokyo, Japan) with the following parameters: tube voltage, 150 kVp; tube current, 12 mAs; and slice thickness, 3 mm. The 2D CT cross-sections and subsequently reconstructed 3D images of the lungs were obtained using a 3D imaging software (Rapidia; Infinitt, Seoul, Korea), and CT cross-sections were displayed in the lung window (window width, 2000; window level, –500). For all CT procedures, the pigs were under general anesthesia and placed in the prone position on the CT table. Anesthesia was induced by an intravenous injection of 4 mg/kg propofol (Provive™, Myungmoon Pharm. Co. Ltd, Seoul, Korea) and maintained by 1.5 MAC isoflurane inhalation (Terrell™, Piramal Healthcare, Bethlehem, PA, USA). All CT images were acquired during a single breath-hold. The CT scans were interpreted by two expert radiologists (from the Ian Animal Diagnostic Imaging Center) who were blinded to the experimental groups.

For quantification of HU values that reflected lung densities and the area ratio of right to left lung lobes, transverse section CT images were selected at the following levels of these four regions: base of the heart, tracheal carina, apex of the heart, and the gastric fundus. The HU values obtained were calculated using following formula:

$$\text{R/L HU value}(\%) = \frac{(\text{Left lobe HU}) - (\text{Right lobe HU})}{(\text{Left lobe HU})} \times 100,$$

representing the HU value as the percentage of irradiated right lung lobe compared with the non-irradiated left lung lobe in the same animal (R/L HU value). The area ratio of right to left lung lobes in

CT cross-sections was quantified and expressed as the area of irradiated right lung lobe divided by that of the non-irradiated left lung lobe, which reflected changes in the size of the right lung lobe in the same animal. In order to quantify the degree of right deviation of the heart and lung, the measurement method of cardiac lateral shift used by Saleh *et al.* [44] was slightly modified and adapted for our study. The maximum lateral distances of the left (LD_L) and right (LD_R) cardiac borders were measured perpendicular to the midline (sterno–spinal line) at the level of the cardiac apex, and then the cardiac right lateral shift was calculated with the following formula:

$$\text{Cardiac right lateral shift}(\%) = \frac{LD_R}{LD_L + LD_R} \times 100,$$ which represented the mediastinal shift to the right side due to fibrosis in the irradiated right lung lobes.

Peripheral blood cell analysis

After anesthesia, blood (200 μl) was collected from the ear vein into ethylenediaminetetraacetic acid tubes and a heparin tube. The WBC count was obtained using a veterinary hematology analyzer (Hemavet 950; CDC Technologies, Oxford, CT, USA), and an automatic dry-type chemistry analyzer (FUJI DRI-CHEM 4000i; FUJI PHOTO FILM Co., Japan) was used for plasma lactate dehydrogenase (LDH) tests.

Broncho-endoscopic findings

All endoscopic evaluations were performed under anesthesia. Endoscopic examination of the irradiated bronchus using fiber-optic endoscopy (Pentax EG-2730 K, Japan) was performed at 6 weeks and 12 weeks after irradiation. Gross changes were evaluated by independent endoscopists. Sterile normal saline (10 ml) was instilled into the lungs, and then the fluid was aspirated into a sterile container. The cells in the bronchoalveolar lavage fluid (BALF) were counted using a hemacytometer.

Histopathological findings

At 22 weeks after irradiation, minipigs were anesthetized, euthanized and necropsied. Lung tissue samples were embedded in paraffin after 24 h fixation with 4% paraformaldehyde; 4-μm thick sections were cut and stained with hematoxylin and eosin (H&E) to assess microscopic findings, or with Masson's Trichrome stain to visualize collagen deposition. The extent of pulmonary fibrosis was quantified using a modified Ashcroft histopathology scoring system [45].

Statistical analysis

Continuous variables were summarized as the mean ± standard deviation (SD). A paired *t*-test was used to determine statistically significant differences in outcomes before and after irradiation. The correlation between selected parameters was analyzed using Spearman's rank correlation analysis, and results were expressed as a correlation coefficient (ρ) with 95% confidence intervals (CI). Regression analyses were used to assess the association between fibrosis score and the three quantified CT parameters. A *P* value less than 0.05 was considered to be statistically significant. Due to the exploratory nature of this study, *P*-values were reported without multiplicity adjustments. All statistical analyses were performed using the statistical program SPSS Statistics 22 (IBM, Armonk, NY, USA).

RESULTS
Thoracic CT findings

Thoracic CT findings after irradiation revealed increased intensities in peribronchial areas and thickening of the interlobular septa and the peribronchial region. Increased opacities and volume loss of irradiated lung lobes were also seen on CT sections (Fig. 1A).

The R/L HU value was calculated as a measure of lung density increase in lung injury. The normal (mean ± SD) R/L HU value in irradiated minipigs was 2.66 ± 0.23% (range: 2.50–3.00%). We assessed the time-course of the R/L HU value at 6, 12, 17 and 22 weeks after radiation exposure (Fig. 1B). The R/L HU ratio was increased, beginning 6 weeks after irradiation (*P* = 0.035, 0.047, 0.021 and 0.020 at 6, 12, 17 and 22 weeks, respectively). The increase of the R/L HU ratio in the irradiated pigs reached a maximum at 6 weeks, then decreased, but remained higher than the R/L HU values of the control group.

The R/L lung area ratio was used to measure the lung volume decrease due to lung injury caused by irradiation. The normal (mean ± SD) R/L lung area ratio in irradiated minipigs was 1.16 ± 0.18 (range: 0.95–1.36). We assessed the time-course of the R/L lung area ratio at 6, 12, 17 and 22 weeks after irradiation (Fig. 1B). The R/L lung area ratio was decreased, beginning at 12 weeks, and a significant decrease was observed at 22 weeks after irradiation (*P* = 0.033).

Cardiac right lateral shift was evaluated to determine the degree of anatomical deviation of the heart and lung resulting from radiation-induced injury. The normal (mean ± SD) cardiac right lateral shift in irradiated minipigs was 46.29 ± 3.89% (range: 41.61–51.03%). We assessed the time-course of the cardiac right lateral shift at 6, 12, 17 and 22 weeks after irradiation (Fig. 1B). The cardiac right lateral shift was significantly increased, beginning 17 weeks after irradiation (*P* = 0.008 and 0.019 at 17 and 22 weeks).

Peripheral blood analysis

WBC counts and plasma LDH levels are often increased in pneumonitis. Thus, we measured peripheral WBC counts and LDH levels at 6, 12, 17 and 22 weeks after irradiation of the minipigs. Compared with normal values, WBC counts of the irradiated minipigs were significantly increased at 6 weeks post irradiation (*P* = 0.029) and partially returned to normal, beginning 17 weeks post irradiation (Fig. 2A). In addition, plasma LDH levels were also increased at 6 and 12 weeks (*P* = 0.013 and 0.016, respectively) and recovered after 17 weeks post irradiation (Fig. 2C). Furthermore, to explore a potential time relationship between HU values and WBC counts or LDH levels, the correlation was examined at the 6, 12, 17 and 22 week time-points after irradiation. Changes in the HU values showed a strong correlation with LDH levels (Spearman's correlation coefficient = 0.868 [95% CI: 0.691–0.947]) (Fig. 2D) and a moderate correlation with the WBC counts (Spearman's correlation coefficient = 0.589 [95% CI: 0.198–0.818]) (Fig. 2B).

Bronchoscopic evaluation and BALF analysis

Bronchoscopic examination was performed to evaluate inflammation and irregularities of the lungs at 6 and 12 weeks post irradiation. We confirmed normal bronchial trees in the irradiated lungs by CT (Fig. 3A) and did not observe any gross lesions (Fig. 3B); however, the BALF from irradiated animals showed an increase in the numbers

A

| Control | 25 Gy | 30 Gy |
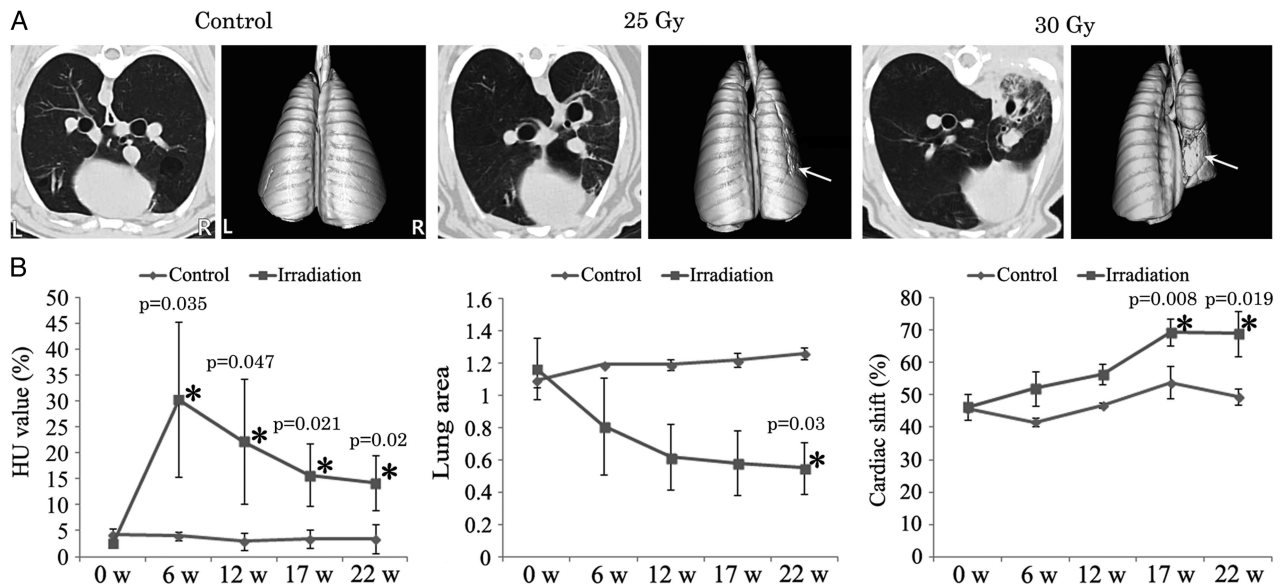
Fig. 1. Time-course evaluation of thoracic computed tomography (CT) in control, and 25 and 30 Gy irradiation groups. (A) Representative images of thoracic CT scans of non-irradiated and irradiated lungs. Note thickening of the interlobular septa and peribronchial regions, increased parenchymal opacifications, and architectural distortion of lung lobes in irradiated right lungs along with cardiac right lateral shift. Arrows indicate lung volume loss in non-irradiated or irradiated lungs reconstructed from thoracic CT scans. (B) Quantitative data obtained from thoracic CT scans regarding HU value (left), lung area ratio (middle), and cardiac right lateral shift (right). Hemi-thoracic irradiation to the lungs induced significant changes in the three quantitative CT parameters. HU values peaked at 6 weeks, and lung area steadily decreased in a time-dependent manner; cardiac right lateral shift was significantly increased after 17 weeks. Data are expressed as the mean ± SD ($n = 2$ in control, $n = 4$ in irradiation). *$P < 0.05$ vs normal value.

of WBCs, neutrophils and lymphocytes (Fig. 3C) compared with the control animals at 6 and 12 weeks, suggesting increased pulmonary inflammation.

Histopathological findings for lung fibrosis

In control lungs, collagen was present in the interlobular septa, and the lobularity was well developed. However, in the irradiated lungs, thickened alveolar walls and widening of the interlobular septa with fibrotic changes were observed (Fig. 4A). Dense fibrosis was noted, mainly in the interlobular septum rather than in the interstitium of the alveolar space, and was more prominent in the 30-Gy–irradiated lungs than in the 25-Gy–irradiated lungs. Moreover, modified Ashcroft scores were significantly increased in the irradiated right lungs of the 25 and 30 Gy groups compared with the control group (Fig. 4B); within the irradiated groups, the modified Ashcroft scores were higher in 30-Gy–irradiated lungs compared with the 25-Gy–irradiated lungs.

Correlation analysis between histological fibrosis score and quantitative CT parameters

Thoracic CT findings at 22 weeks after irradiation revealed characteristics of lung fibrosis (Fig. 1A). Lungs exposed to 30 Gy showed homogeneously increased opacities in the right upper lobes, which were sharply demarcated from the other lobes. Volume loss of the right lung lobes was also confirmed by 3D reconstructed images of the lungs (Fig. 3A).

Quantification of R/L HU values at 22 weeks after hemithoracic irradiation showed a significant increase in the R/L HU compared with in the control group (Fig. 1B), and the 30-Gy group showed a greater increase than the 25-Gy group (Fig. 5A). The R/L area ratio was significantly decreased in irradiated animals 22 weeks after irradiation (Fig. 1B), and the 30-Gy group showed a lower R/L area ratio than the 25-Gy group (Fig. 5A). The cardiac right lateral shift was significantly increased in irradiated animals 22 weeks after irradiation (Fig. 1B), and was greater in the 30-Gy group than in the 25-Gy group (Fig. 5A).

The modified Ashcroft fibrosis scores and quantitative CT parameters at 22 weeks post irradiation were plotted to explore a potential correlation. Changes in the modified Ashcroft fibrosis scores showed a strong correlation with the R/L HU values and the cardiac right lateral shift (Spearman's correlation coefficients were 0.886 [95% CI: 0.264–0.987] and 0.943 [95% CI: 0.559–0.994], respectively) and a strong inverse correlation with the R/L area ratio (Spearman's correlation coefficient was 0.886 (95% CI: 0.264–0.987)) (Fig. 5B).

DISCUSSION

The minipig is emerging as an alternative large animal model for characterizing acute radiation syndrome (ARS) [3, 33, 34], and we are evaluating the minipig as an RILI model. Animal models should show similarities in lung radiation dose responses and time-courses to those seen in humans [1]. The radiation doses for RILI in rats were in the range of 10–15 Gy to the whole thorax or 25–28 Gy to the
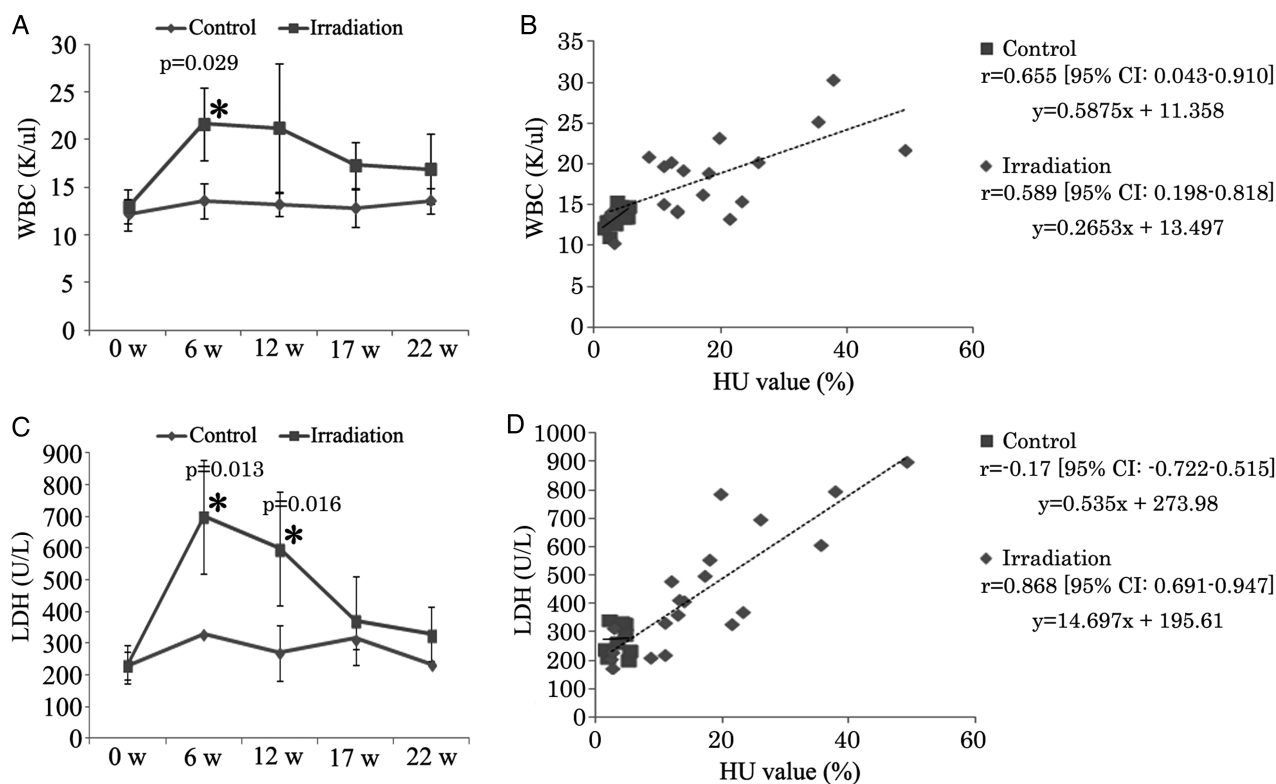
Fig. 2. Time-course evaluation of pneumonitis in control and irradiation groups. (A) WBC counts peaked at 6 weeks and decreased after 17 weeks. Data are expressed as the mean ± SD (n = 2 in control, n = 4 in irradiation). *P < 0.05 vs normal value. (B) Correlation analysis of WBC counts compared with HU value (the Spearman's correlation coefficients were 0.655 [95% CI: 0.043–0.910] in control and 0.589 [95% CI: 0.198–0.818] in irradiation) (n = 10 in control, n = 20 in irradiation, 5 time-points per animal). P < 0.05 was considered statistically significant. (C) Plasma LDH peaked at from 6–12 weeks and decreased after 17 weeks. Data are expressed as the mean ± SD (n = 2 in control, n = 4 in irradiation). *P < 0.05 vs normal value. (D) Correlation analysis of plasma LDH compared with HU value (the Spearman's correlation coefficients were –0.17 [95% CI: −0.722–0.515] in control and 0.868 [95% CI: 0.691–0.947] in irradiation) (n = 10 in control, n = 20 in irradiation, 5 time-points per animal). P < 0.05 was considered statistically significant.

hemithorax [46–48]. Pneumonitis developed ~2–4 months post irradiation [5], whereas fibrosis was seen at 4–6 months post irradiation [49]. In order to investigate dose responses and time-courses for the development of pneumonitis and fibrosis, we designed a strategy for irradiating the right hemithorax rather than the whole thorax, which was expected to reduce mortality, thereby allowing a long-term study of the development of lung fibrosis in the late phase, and permitting each animal to act as its own control [7].

Because we couldn't observe obvious histological changes until 30 weeks after irradiation of <20 Gy to the hemithorax in the preliminary study (data was not shown) and other researchers have successfully used RILI rats models with over 25 Gy to the hemithorax [46–48], in the current study we chose the irradiation dose as 25 or 30 Gy for effective induction of pneumonitis and lung fibrosis. Most of the spectra of changes seen on thoracic CT of radiotherapy-induced fibrosis in human lungs were also identified in our minipig model. However, the radiological interpretation of the CT findings in humans was limited, because the findings were largely qualitative and needed refinement. Thus, we measured numerical values easily obtainable from CT

images to allow more rapid, quantitative assessment of RILI. The first parameter that we used was the HU value. The HU value reflects lung density and has been investigated by several groups using chest CT [33, 50–52]. We translated the HU values into a ratio of irradiated right to normal left lung lobes, and through this translation method (in addition to determining lung density), we were able to adjust the HU measurements to account for individual variations. The second parameter was the lung area ratio of the transverse CT section. The lung area ratio was determined from measurements of four regions as described in the Materials and Methods, and is thought to reflect changes in the size of the lung lobes induced by the various radiation doses. The last CT parameter that we adapted was the degree of cardiac right lateral shift. The heart is the largest mediastinal organ, and a decrease in lung volume due to lung fibrosis results in its anatomical deviation toward the affected lung [53, 54]. All of these CT parameters (increased opacities, lung volume loss, and mediastinal shifting to the irradiated side) efficiently demonstrated that pneumonitis developed at ~6–12 weeks post irradiation, whereas fibrosis was observed 22 weeks post irradiation onwards.
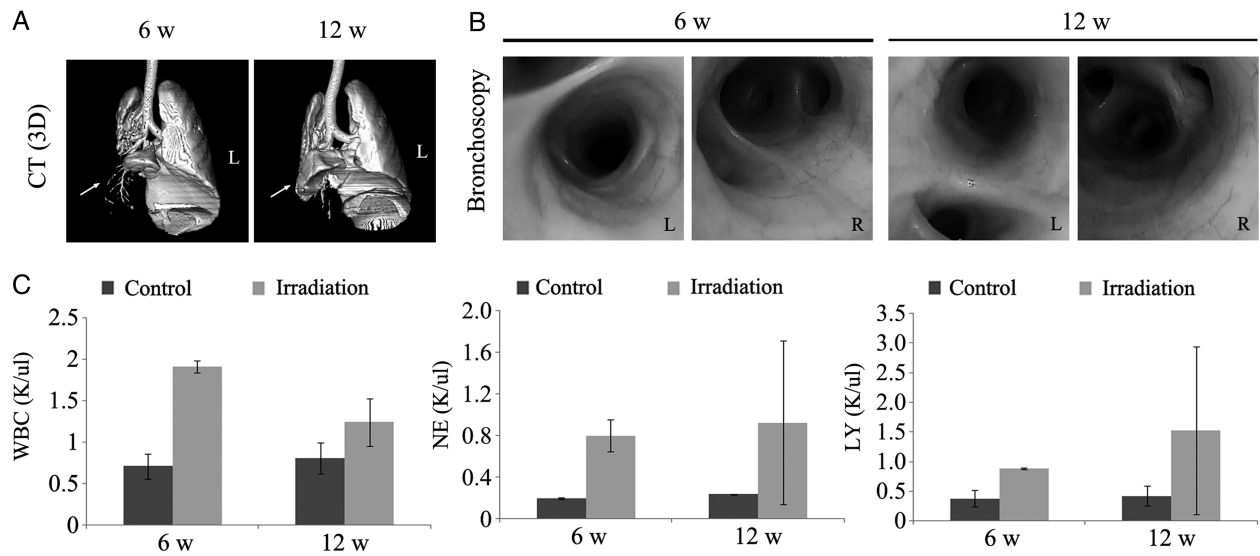
Fig. 3. Bronchoscopic evaluation of pneumonitis at 6 and 12 weeks in 30 Gy-irradiated animals. (A) Representative 3D images of 30 Gy-irradiated lungs reconstructed from thoracic CT scans. The irradiated lung lobe showed consolidation, although normal bronchial trees were observed. (B) Gross evaluation by bronchoscopy. The irradiated lung did not show any gross lesions upon bronchoscopic evaluation. (C) Numbers of WBCs (left), neutrophils (middle) and lymphocytes (right) in BALF. The BALF WBC, neutrophil, and lymphocyte counts were much higher in the irradiated groups compared with in the control group. Data are expressed as the mean ± SD ($n = 2$).
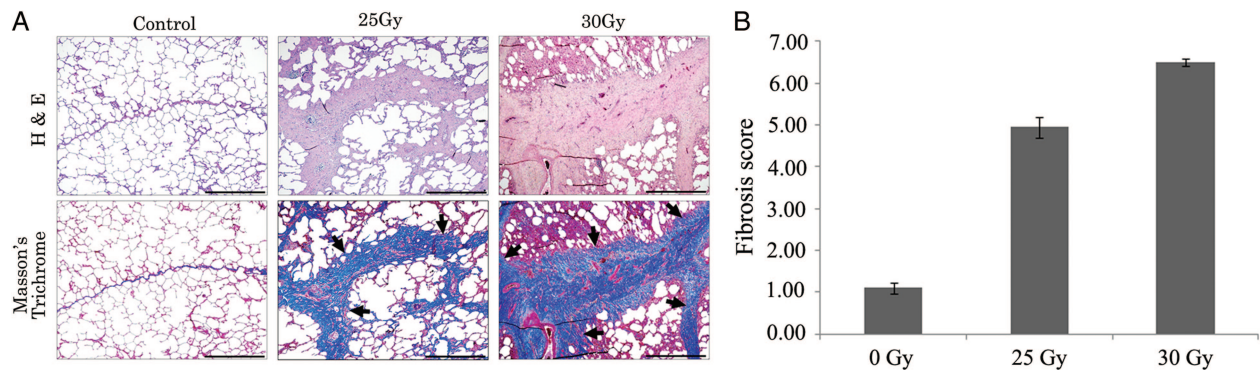
Fig. 4. Histopathologic evaluation of right lung lobe tissues in control, 25 Gy, and 30 Gy groups at 22 weeks post irradiation. (A) Representative images of H&E and Masson's Trichrome stains of non-irradiated and irradiated right lungs. Note that the thickening of interlobular septa with collagenous tissue (arrows) was more severe in the 30 Gy group than in the 25 Gy group. Scale bar represents 1 mm (right bottom). (B) Quantitative fibrosis scores of non-irradiated and irradiated right lungs using the modified Ashcroft fibrosis scoring system. Hemi-thoracic irradiation increased fibrosis grade in a dose-dependent manner. Data are expressed as the mean ± SD ($n = 2$).

To confirm the presence of pneumonitis, we used clinical diagnostic methods, including: complete blood count, bronchoscopy, and BALF cytology. WBC counts and LDH levels in the peripheral blood of irradiated animals peaked at 6 weeks ($P = 0.029$ and 0.013, respectively), and changes in the plasma LDH showed a strong correlation with the HU values. BALF cytology also showed an increase in the number of WBCs, neutrophils and lymphocytes at 6 and 12 weeks post irradiation. However, we did not observe any inflammation or irregularities in the bronchial trees upon bronchoscopic evaluation.

To confirm fibrosis-related findings by CT, histopathological analysis was performed. The most characteristic histological feature of fibrosis observed was thickening of the interlobular septa with dense collagenous tissue. Our histological findings regarding lung fibrosis in the minipigs were in agreement with those of other investigators, who have demonstrated interlobular septal thickening induced by irradiation in swine lungs [7, 36, 55]. The heterogeneous distribution of thickened alveolar walls, further restricted by widening of the interlobular septa due to dense fibrosis, would render the alveoli unable to function normally; this distinctive pattern of fibrosis may explain the
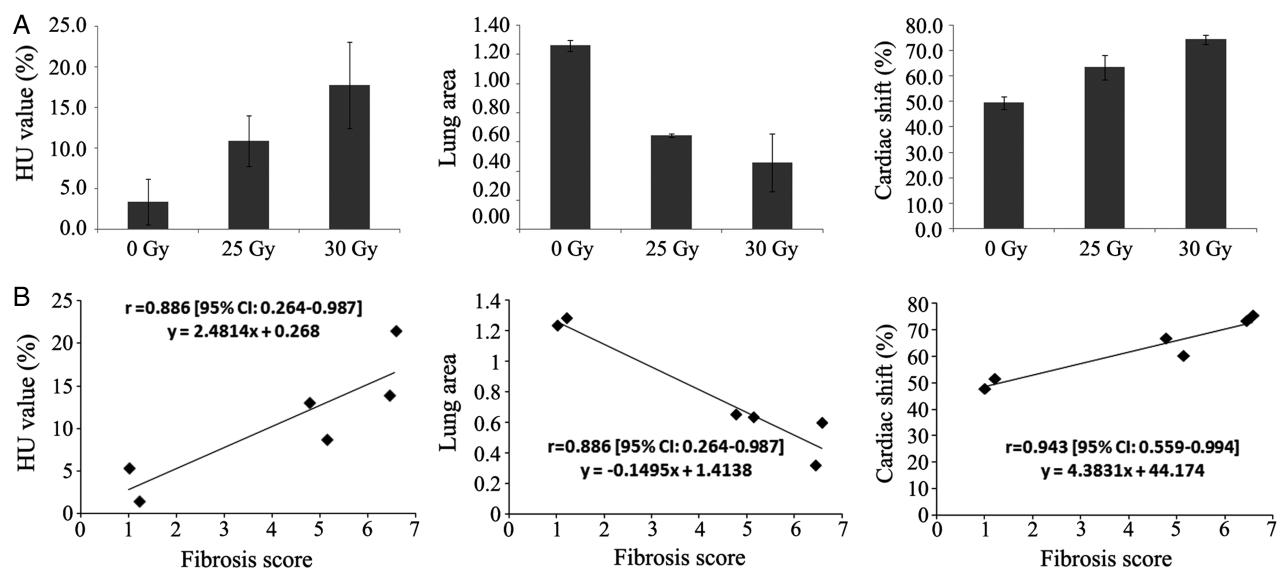
Fig. 5. Thoracic computed tomography (CT) of non-irradiated or irradiated lungs in control, 25 Gy, and 30 Gy groups at 22 weeks post irradiation (IR). (A) Quantitative data obtained from thoracic CT scans regarding HU value (left), lung area ratio (middle) and cardiac right lateral shift (right). Hemi-thoracic irradiation to the lungs induced dose-dependent changes in three quantitative CT parameters. Data are expressed as the mean ± SD ($n = 2$). (B) Correlation analysis of quantitative CT parameters to histological fibrosis score. Three quantified CT parameters (HU value, lung area and cardiac right lateral shift) were strongly and significantly correlated to modified Ashcroft fibrosis scores (the Spearman's correlation coefficients were 0.886 [95% CI: 0.264–0.987], 0.886 [95% CI: 0.264–0.987] and 0.943 [95% CI: 0.559–0.994], respectively) ($n = 6$).

greater radiosensitivity observed in the lungs of pigs, and indeed humans, as compared with rodents after a single high-dose exposure to radiation [7].

Lastly, we demonstrated strong and significant correlations between the histological fibrosis scores measured by the modified Ashcroft scoring system and our CT parameters. Although this study had limitations due to the small sample size and short follow-up time, the results from the correlation analysis indicated that the three CT parameters obtained from simple 2D sections could quantitatively reflect the severity of lung fibrosis (as did the histological fibrosis scoring method), and without complicated and time-consuming procedures in our swine model.

In conclusion, we established a single high-dose RILI model using minipigs, in which the progression of RILI could be followed via a thoracic CT technique. A major strength of our minipig model and experimental design is that it allows the same animal to serve as both a test and a control subject. Furthermore, by using our three chest CT parameters, investigators can obtain quantifiable clinical data by simple translation methods. As we seek treatment strategies for radiation-induced lung fibrosis, this objective, quantitative technique using chest CT could emerge as a valuable tool for pre-clinical studies.

REFERENCES
1. Williams J-P, Brown S-L, Georges G-E, et al. Animal models for medical countermeasures to radiation exposure. *Radiat Res* 2010;173:557–78.
2. McDonald S, Rubin P, Phillips T-L, et al. Injury to the lung from cancer therapy: clinical syndromes, measurable endpoints, and potential scoring systems. *Int J Radiat Oncol Biol Phys* 1995;31: 1187–203.
3. Browne D, Weiss J-F, MacVittie T-J, et al. Protocol for the treatment of radiation injuries. *Adv Space Res* 1992;12:165–8.
4. Tsoutsou P-G, Koukourakis M-I. Radiation pneumonitis and fibrosis: mechanisms underlying its pathogenesis and implications for future research. *Int J Radiat Oncol Biol Phys* 2006;66:1281–93.
5. Sharplin J, Franko A-J. A quantitative histological study of strain-dependent differences in the effects of irradiation on mouse lung during the early phase. *Radiat Res* 1989;119:1–14.
6. Johnston C-J, Wright T-W, Rubin P, et al. Alterations in the expression of chemokine mRNA levels in fibrosis-resistant and -sensitive mice after thoracic irradiation. *Exp Lung Res* 1998;24:321–37.
7. Hopewell J-W, Rezvani M, Moustafa H-F. The pig as a model for the study of radiation effects on the lung. *Int J Radiat Biol* 2000;76:447–52.
8. Sommerer D, Suss R, Hammerschmidt S, et al. Analysis of the phospholipid composition of bronchoalveolar lavage (BAL) fluid from man and minipig by MALDI-TOF mass spectrometry in combination with TLC. *J Pharm Biomed Anal* 2004;35:199–206.

9. Hotchkiss J-R, Sanders M-H, Clermont G, et al. Preventing "bored-lung disease" when treating patients with ventilatory failure. *Crit Care Med* 2007;35:1797–9.

10. Glenny R-W, Bernard S-L, Luchtel D-L, et al. The spatial-temporal redistribution of pulmonary blood flow with postnatal growth. *J Appl Physiol* 2007;102:1281–8.

11. Bouziri A, Hamdi A, Khaldi A, et al. Management of meconium aspiration syndrome with highfrequency oscillatory ventilation. *Tunis Med* 2011;89:632–7.

12. Budas G-R, Churchill E-N, Mochly-Rosen D. Cardioprotective mechanisms of PKC isozyme-selective activators and inhibitors in the treatment of ischemia-reperfusion injury. *Pharmacol Res* 2007;55:523–36.

13. Schwarzkopf K, Schreiber T, Gaser E, et al. The effects of xenon or nitrous oxide supplementation on systemic oxygenation and pulmonary perfusion during one-lung ventilation in pigs. *Anesth Analg* 2005;100:335–9.

14. Gushima Y, Ichikado K, Suga M, et al. Expression of matrix metalloproteinases in pigs with hyperoxia-induced acute lung injury. *Eur Respir J* 2001;18:827–37.

15. Roch A, Castanier M, Mardelle V, et al. Effect of hypertonic saline pre-treatment on ischemia-reperfusion lung injury in pig. *J Heart Lung Transplant* 2008;27:1023–30.

16. Jayle C, Hauet T, Menet E, et al. Beneficial effects of polyethylene glycol combined with low-potassium solution against lung ischemia/reperfusion injury in an isolated, perfused, functional pig lung. *Transplant Proc* 2002;34:834–5.

17. Pfeiffer S, Zorn G-L 3rd, Zhang J-P, et al. Hyperacute lung rejection in the pig-to-human model. III. Platelet receptor inhibitors synergistically modulate complement activation and lung injury. *Transplantation* 2003;75:953–9.

18. Yokoyama T, Tomiguchi S, Nishi J, et al. Hyperoxia-induced acute lung injury using a pig model: correlation between MR imaging and histologic results. *Radiat Med* 2001;19:131–43.

19. Zetterstrom H, Jakobson S, Janeras L. Influence of plasma oncotic pressure on lung water accumulation and gas exchange after experimental lung injury in the pig. *Acta Anaesthesiol Scand* 1981;25:117–24.

20. Xiao J, Zhong R, Shi S-Y, et al. [An investigation of the protective effect of prostaglandin E1 liposome on acute lung injury in pig]. *Zhongguo Wei Zhong Bing Ji Jiu Yi Xue* 2008;20:345–8.

21. Moroni M, Ngudiankama B-F, Christensen C, et al. The Gottingen minipig is a model of the hematopoietic acute radiation syndrome: G-colony stimulating factor stimulates hematopoiesis and enhances survival from lethal total-body γ-irradiation. *Int J Radiat Oncol Biol Phys* 2013;86:986–92.

22. Shim S, Jang W-S, Lee S-J, et al. Development of a new minipig model to study radiation-induced gastrointestinal syndrome and its application in clinical research. *Radiat Res* 2014;181: 387–95.

23. Agay D, Scherthan H, Forcheron F, et al. Multipotent mesenchymal stem cell grafting to treat cutaneous radiation syndrome: development of a new minipig model. *Exp Hematol* 2010;38: 945–56.

24. Chen C, Yan L-M, Guo K-Y, et al. The diagnostic value of 18F-FDG-PET/CT in hematopoietic radiation toxicity: a Tibet minipig model. *J Radiat Res* 2012;53:537–44.

25. Moroni M, Coolbaugh T-V, Lombardini E, et al. Hematopoietic radiation syndrome in the Gottingen minipig. *Radiat Res* 2011;176: 89–101.

26. Riccobono D, Forcheron F, Agay D, et al. Transient gene therapy to treat cutaneous radiation syndrome: development in a minipig model. *Health Phys* 2014;106:713–9.

27. Forcheron F, Agay D, Scherthan H, et al. Autologous adipocyte derived stem cells favour healing in a minipig model of cutaneous radiation syndrome. *PLoS One* 2012;7:e31694.

28. Wang R-S, Zhang T-T, Xu Z-H, et al. Injury in minipig parotid glands following fractionated exposure to 30 Gy of ionizing radiation. *Otolaryngol Head Neck Surg* 2014;151:100–6.

29. Radfar L, Sirois D-A. Structural and functional injury in minipig salivary glands following fractionated exposure to 70 Gy of ionizing radiation: an animal model for human radiation-induced salivary gland injury. *Oral Surg Oral Med Oral Pathol Oral Radiol Endod* 2003;96:267–74.

30. Travis E-L, Vojnovic B, Davies E-E, et al. A plethysmographic method for measuring function in locally irradiated mouse lung. *Br J Radiol* 1979;52:67–74.

31. Hong J-H, Chiang C-S, Tsao C-Y, et al. Rapid induction of cytokine gene expression in the lung after single and fractionated doses of radiation. *Int J Radiat Biol* 1999;75:1421–7.

32. Johnston C-J, Piedboeuf B, Rubin P, et al. Early and persistent alterations in the expression of interleukin-1 alpha, interleukin-1 beta and tumor necrosis factor alpha mRNA levels in fibrosis-resistant and sensitive mice after thoracic irradiation. *Radiat Res* 1996;145:762–7.

33. Karimi R, Tornling G, Forsslund H, et al. Lung density on high resolution computer tomography (HRCT) reflects degree of inflammation in smokers. *Respir Res* 2014;15:23.

34. Libshitz H-I, Shuman L-S. Radiation-induced pulmonary change: CT findings. *J Comput Assist Tomogr* 1984;8:15–9.

35. Liao Z-X, Travis E-L, Tucker S-L. Damage and morbidity from pneumonitis after irradiation of partial volumes of mouse lung. *Int J Radiat Oncol Biol Phys* 1995;32:1359–70.

36. Takahashi M, Balazs G, Pipman Y, et al. Radiation-induced lung injury using a pig model. Evaluation by high-resolution computed tomography. *Invest Radiol* 1995;30:79–86.

37. Long F-R. High-resolution computed tomography of the lung in children with cystic fibrosis: technical factors. *Proc Am Thorac Soc* 2007;4:306–9.

38. Langton Hewer S-C. Is limited computed tomography the future for imaging the lungs of children with cystic fibrosis? *Arch Dis Child* 2006;91:377–8.

39. Kuhnigk J-M, Dicken V, Zidowitz S, et al. Informatics in radiology (infoRAD): new tools for computer assistance in thoracic CT. Part 1. Functional analysis of lungs, lung lobes, and bronchopulmonary segments. *Radiographics* 2005;25:525–36.

40. Mets O-M, de Jong P-A, van Ginneken B, et al. Quantitative computed tomography in COPD: possibilities and limitations. *Lung* 2012;190:133–45.

41. Guo Y, Zhou C, Chan H-P, et al. Automated iterative neutrosophic lung segmentation for image analysis in thoracic computed tomography. *Med Phys* 2013;40:081912.

42. Bitter I, Van Uitert R, Wolf I, et al. Comparison of four freely available frameworks for image processing and visualization that use ITK. *IEEE Trans Vis Comput Graph* 2007;13:483–93.

43. Park S-C, Leader J-K, Tan J, et al. Separation of left and right lungs using 3-dimensional information of sequential computed tomography images and a guided dynamic programming algorithm. *J Comput Assist Tomogr* 2011;35:280–9.

44. Saleh R-S, Finn J-P, Fenchel M, et al. Cardiovascular magnetic resonance in patients with pectus excavatum compared with normal controls. *J Cardiovasc Magn Reson* 2010;12:73.

45. Hubner R-H, Gitter W, El Mokhtari N-E, et al. Standardized quantification of pulmonary fibrosis in histological samples. *Biotechniques* 2008;44:507–11, 14–7.

46. van Rongen E, Tan C, Zurcher C. Early and late effects of fractionated irradiation of the thorax of WAG/Rij rats. *Br J Cancer Suppl* 1986;7:333–5.

47. Zhang R, Ghosh S-N, Zhu D, et al. Structural and functional alterations in the rat lung following whole thoracic irradiation with moderate doses: injury and recovery. *Int J Radiat Biol* 2008;84:487–97.

48. Pauluhn J, Baumann M, Hirth-Dietrich C, et al. Rat model of lung fibrosis: comparison of functional, biochemical, and histopathological changes 4 months after single irradiation of the right hemithorax. *Toxicology* 2001;161:153–63.

49. Sharplin J, Franko A-J. A quantitative histological study of strain-dependent differences in the effects of irradiation on mouse lung during the intermediate and late phases. *Radiat Res* 1989;119: 15–31.

50. Biernacki W, Redpath A-T, Best J-J, et al. Measurement of CT lung density in patients with chronic asthma. *Eur Respir J* 1997;10:2455–9.

51. Diot Q, Marks L-B, Bentzen S-M, et al. Comparison of radiation-induced normal lung tissue density changes for patients from multiple institutions receiving conventional or hypofractionated treatments. *Int J Radiat Oncol Biol Phys* 2014;89:626–32.

52. Niehues S-M, Muller C, Plendl J, et al. The effect of prone versus supine positioning of Goettingen minipigs on lung density as viewed by computed tomography. *Clin Hemorheol Microcirc* 2012;52:85–92.

53. Park K-J, Chung J-Y, Chun M-S, et al. Radiation-induced lung disease and the impact of radiation methods on imaging features. *Radiographics* 2000;20:83–98.

54. Choi Y-W, Munden R-F, Erasmus J-J, et al. Effects of radiation therapy on the lung: radiologic appearances and differential diagnosis. *Radiographics* 2004;24:985–97; discussion 98.

55. Herrmann T, Baumann M, Voigtmann L, et al. Effect of irradiated volume on lung damage in pigs. *Radiother Oncol* 1997;44: 35–40.